Plasma Chem Plasma Process (2013) 33:725–735
DOI 10.1007/s11090-013-9455-7

ORIGINAL PAPER

Plasma-Assisted Synthesis of TiO_2 Nanorods by Gliding Arc Discharge Processing at Atmospheric Pressure for Photocatalytic Applications

E. Acayanka · A. Tiya Djowe · S. Laminsi · C. C. Tchoumkwé · S. Nzali · A. Poupi Mbouopda · P. T. Ndifon · E. M. Gaigneaux

Received: 21 February 2013 / Accepted: 24 April 2013 / Published online: 10 May 2013

Abstract The present study explores a new method of synthesis of TiO_2 nano-particles in an aqueous medium from $TiCl_3$ precursor by non-thermal plasma in humid air as feeding gas obtained at atmospheric pressure. The precursor solution, $TiCl_3$ is oxidized by strongly reactive species generated by gliding arc plasma ($HO^{\cdot} = 2.85$ V/SHE) to produce titanium oxide powders. The synthesized powder was characterised by X-ray powder diffraction, scanning electron microscopy, transmission electron microscopy, FTIR spectroscopy, nitrogen physisorption, and UV–Vis spectroscopy. The results obtained showed that the material consists of rod-shaped nanoparticles of rutile and anatase phases. The presence of TiO_2 phases was confirmed by FTIR spectrum and textural analyses showed that the material is mesoporous with specific surface area of 158 $m^2\ g^{-1}$. UV–Visible spectrum of the plasma-synthesized TiO_2 sample showed that it absorbs in the UV–A region leading to effective use as a photocatalyst under visible light.

Keywords Non-thermal plasma · Gliding arc discharge · Nanorods · Titanium dioxide · Photocatalyst

E. Acayanka · A. Tiya Djowe · S. Laminsi (✉) · C. C. Tchoumkwé · A. Poupi Mbouopda · P. T. Ndifon
Inorganic Chemistry Department, University of Yaoundé I, P.O. Box 812, Yaoundé, Cameroon
e-mail: s.laminsi@yahoo.fr

E. Acayanka
Instituto de Química, Universidade Federal do Rio Grande do Sul, Av. Bento Gonc, Alves 9500, Caixa Postal 15003, Porto Alegre, RS CEP 91501-970, Brazil

A. Tiya Djowe · E. M. Gaigneaux
Institute of Condensed Matter and Nanosciences (IMCN), Division "Molecules, Solids and reactiviTy" (MOST), Université catholique de Louvain, Croix du Sud 2/L7.05.17, Louvain-la-Neuve 1348, Belgium

S. Nzali
School of Wood, Water and Natural Resources, Faculty of Agronomy and Agricultural Sciences, University of Dschang (Ebolowa campus), P.O. Box 786, Ebolowa, Cameroon

Introduction

The demand for photocatalytic systems activated by sunlight is increasing rapidly. Recently a lot of efforts have been made to develop efficient visible light-activated photocatalysts. The development of photocatalysts activated by visible light would have an impact and would lead to many applications of practical relevance to society. Consequently, the current research efforts are directed towards shifting the optical response of photocatalysts to the visible spectrum of solar radiation. Among the photocatalytic semiconductors studied, titanium oxide-based catalysts offer certain specific advantages. The band gap of TiO_2 is about 3.2 eV (corresponding to a wavelength of about 380 nm) and can be shifted to the visible region by suitable doping.

Titanium dioxide, particularly in the anatase form, is a photocatalyst under ultraviolet (UV) light. Recently it has been found that titanium dioxide, when spiked with nitrogen ions or doped with metal oxide, is also a photocatalyst under either visible or UV–A light, i.e. the UV range with the wavelength between 315 and 400 nm ($315\ nm < \lambda < 400\ nm$) [1]. The anatase form is characterized by a desirable tenfold higher photochemical activity than rutile because it is provided with a special electronic structure that prevents "internal short circuits".

Many approaches have been used to modify the TiO_2 semiconductor for its use in the visible light photocatalysis. Doping of titanium oxide with aliovalent oxides has been attempted in order to develop photocatalytic materials active in visible light. However, the photocatalytic activity of metal doping is impaired by thermal instability and an increase in the recombination rate of photogenerated electrons and holes [2]. Recently our laboratory developed a new method to synthesize nanocrystalline titania involving oxidation of $TiCl_3$ by Gliding arc plasma. Gliding arc plasma is a novel technique that takes its advantage to the presence of auto-generated reactive species like $HO^{\cdot}$ and $NO^{\cdot}$ radicals. The gliding electric discharge is obtained by blowing an electric arc burning between diverging electrodes by axial gas flow [3]. The plasma device was recently used for the abatement of gaseous or liquid chemical pollutants [4–8]. When humid air is selected as the ambient gas for discharges at atmospheric pressure, the resulting plasma was found highly efficient for oxidizing because the resulting non-thermal plasma formed involves $HO^{\cdot}$ as a result of electron (or/and photon) impact dissociation of water molecules present in the ambient gas [9]. The thermal energy available in the arc enables the energy transfer to the ambient molecules or the "parent species", and thus favours the breaking of H–OH and O=O bonds. This feature requires less energy than $N \equiv N$ breaking and allows the rising of gaseous moieties to excited states from their fundamental energy level.

Thus the $NO^{\cdot}$ and $HO^{\cdot}$ radicals mainly formed in the arc will be the determining agents for the chemical reactions observed in the target solution. The formation of $HO^{\cdot}$ and $NO^{\cdot}$ as the main products is confirmed by spectroscopy measurements and results from electron impact on water (Eqs. 1, 2).

$$H_2O + e^- \rightarrow H^{\cdot} + HO^{\cdot} + e^- \quad (1)$$

$$H_2O + e^- \rightarrow H^+ + HO^{\cdot} + 2e^- \quad (2)$$

$$O_2 + e^- \rightarrow 2O + e^- \quad (3)$$

$$N_2 + O \rightarrow NO^{\cdot} + N \quad (4)$$

These primary species will then react both with themselves and the parent species to form secondary species according to the following main side reactions in the gas phase

$$N + O \rightarrow NO^{\cdot} \quad (5)$$

$$O_2 + O + M \rightarrow O_3 + M \quad (6)$$

$$O_3 + HO^{\cdot} \rightarrow O_2 + HO_2^{\cdot} \quad (7)$$

$$O_3 + NO^{\cdot} \rightarrow NO_2 + O_2 \quad (8)$$

$$NO_2 + OH^{\cdot} \rightarrow ONO_2H \quad (9)$$

The reactive radicals $OH^{\cdot}$ and $NO^{\cdot}$ react both with themselves and the parent species forming the ambient atmosphere (i.e., O_2, N_2, H_2O) and are thus present in the quenched plasma plume, so that the impinging active species falling on the liquid surface are mainly H_2O_2 and nitrogen oxides.

$$2\ OH^{\cdot} \rightarrow H_2O_2 \quad (10)$$

$$OH^{\cdot} + O^{\cdot} \rightarrow NO_2 \quad (11)$$

$$NO_2 + OH^{\cdot} \rightarrow ONOOH \quad (12)$$

$$ONO_2H \rightarrow NO_3^{-} + H^{+} \quad (13)$$

$NO^{\cdot}$ is responsible for the formation of nitrous acid (via NO_2) which disproportionates into $NO^{\cdot}$ and NO_3^{-} in acidic solution but also yields peroxynitrous acid HNOOH which later izomerizes in nitrate ions. The major advantages of the gliding arc plasma technique include short processing time, and low cost. The process can also be customised to synthesise any desired product and the technique is ideally suited for large-scale production.

The present paper reports the experimental method adopted to synthesize nanocrystalline TiO_2 powder from titanium salt solution via gliding arc plasma at low temperature. X-ray powder diffraction (XRD), transmission electron microscopy (TEM), scanning electron microscopy (SEM), nitrogen physisorption and Fourier transform-infrared spectroscopy (FTIR) were used to characterize the synthesized powder. Photocatalytic activity of the product was evaluated by diffuse reflectance ultraviolet–visible (UV–Vis) spectroscopy.

Experimental Method

Plasma Reactor for the Synthesis of Nanosized TiO_2 Powder

A schematic presentation of the plasma reactor is shown in Fig. 1. It includes a couple of aluminium electrodes symmetrically disposed on both sides of an atomizing nozzle (diameter: 1.5 mm, length: 6 cm) and connected to an AC 220 V/10 kV–1A high voltage transformer which delivers a mean current intensity 160 mA (600 V) in operating conditions ($P \approx 100$ W). The selected feeding gas was water saturated air provided by a compressor and passing through a bubbling flask before entering the reactor. Water–air was sprayed directly into the zone formed between the electrodes through an atomizing nozzle. An arc is formed between the electrodes when a high voltage is applied. The arc is then pushed away by the bi-phase flow from the nozzle and glides along the electrodes until it collapses. The arc length increases on moving and its temperature decreases, so that the arc turns from thermal plasma to quenched plasma on breaking into a plume. A new arc then forms at the narrowest gap and the cycle resumes as a large plasma plume in contact

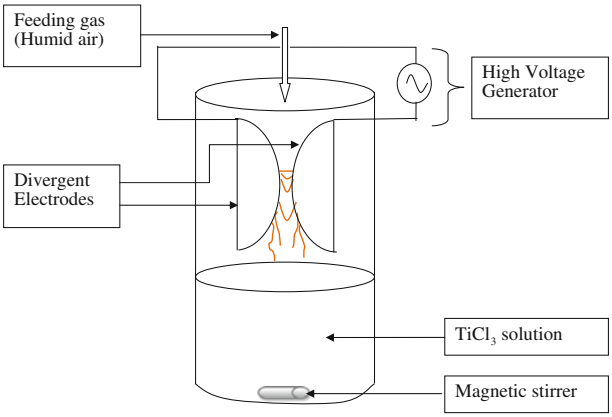

Fig. 1 Scheme showing the experimental setup: transformer (high voltage = 10 kV–1A in open conditions); electrode tips to target distance d = 2.5 cm

Table 1 Typical operating parameters

Arc voltage (V)	600
Arc current (mA)	160
Nozzle diameter (mm)	1.5
Feeding plasma gas	Humid air (O_2, N_2, H_2O)
Flow rate (L h^{-1})	800

with the liquid surface allows chemical reactions to develop. The target solution is thus directly exposed to the plasma plume for time t*(min) [3, 5, 10].

Taking into account that the formation of chemical species in plasma medium requires a complex mechanism and is governed by the gas flow and the quantity of energy provided by the electric source, the typical operating parameters are gathered in Table 1 [11].

Major Chemical Reactions Involved in Humid Air Plasma

The major reactions observed in an aqueous target exposed to humid air plasma are acidification and strong oxidizing effects. They are interpreted as a direct consequence of the formation of $OH^{\cdot}$ and $NO^{\cdot}$ radicals, the major reactive species identified and quantified in the plasma plume by spectrometry studies [12] and recently confirmed [13]. Short life species formed in the discharge may also react in the gas phase with the feed gas molecules O_2, N_2, and H_2O mainly and yield a variety of oxygen and/or nitrogen containing species (e.g., $HO_2^{\cdot}$, H_2O_2 and NOx and their derivatives). Interaction between the electron flux of the discharge and water vapour may also be a source of reactive species such as the $OH^{\cdot}$ radicals in a way similar to that occurring in water radiolysis. The $OH^{\cdot}$ radical is a very powerful oxidizing agent. This innovative technique was successfully used for oxidizing many compounds such as iron(II) complexes [14], azoïc dyes in textile effluents [15], spent solvents [16].

Synthesis and Analysis Procedure

$TiCl_3$ solution used as precursor has been purchased from Merck with analytical grade more than 99.95 % and trace metals basis. The stock solution was prepared by dissolving

accurate weight sample without further purification in de-ionized water to the concentration of 5 mol L^{-1}. The working solutions were obtained by diluting the stock solution to the required concentrations. The target $TiCl_3$ solution (450 mL; 2 mol L^{-1}) was disposed normally to the axis of the water cooled glass reactor (Fig. 1) at a distance of about 50 mm from the electrodes tips. The solution was magnetically stirred. Solutions were exposed to the plasma for different time t* (i.e., 0, 10, 20, 30, 40, 50, and 60 min). After the discharge was switched off, an aliquot of the exposed solution was centrifuged at 3,600 rpm for 10 min, and aliquots of supernatant were immediately analyzed. The variation of the composition of the targeted solution was followed by spectrophotometric investigation. The absorbance measurements were made at the maximum wavelength of titanium chlorure which is 498 nm using a UV–Vis spectrophotometer model Aqualytic Spectro-Direct. It should be pointed out that no colour changes of the $TiCl_3$ solution was observed when these were immersed in aqueous solution ranging from pH 2.0 to 10.0. The resulting TiO_2 was washed several times with deionised water to remove excess $TiCl_3$ and dried in an oven at 109 °C until constant weight. After the stabilisation reached it was kept in glass bottle for further analysis. The concentration of TiO_2 formed after each exposure time was determined gravimetrically.

Characterization

XRD analyses were performed on a Siemens D5000 diffractometer using the Kα radiation of Cu ($\lambda = 1.5$, 418 Å). The ICDD-JCPDS database was used to identify the crystalline phases.

Transmission electron microscopy and SEM were used for determining the size and shape of the powder particles. For TEM, the material was dispersed in butanol and deposited onto a perforated carbon foil supported on a copper grid. The investigations were performed on a Tecnai F30 microscope (field emission cathode, operated at 300 kV). SEM micrographs were taken with a JSM-35C, JEOL SEM.

The Fourier transform-infrared spectroscopy was recorded with Equinox IFS55 spectrometer (Brücker) equipped with a DTGS detector. The absorption spectra were obtained by the recording of 100 scans between 400 and 4,000 cm^{-1} with a resolution of 4 cm^{-1}. The powders were diluted in analytical grade KBr 99 % (2 mg of TiO_2 for 200 mg of KBr) and then pressed into self-supporting disks before analysis.

Textural analyses were carried out on Micromeritics Tristar 3000 equipment using N_2 adsorption/desorption at −196 °C. Before measurement, the samples were outgassed at 150 °C overnight under vacuum. The specific surface area and pore size were respectively calculated using BET equation [15] and BJH method [16].

Diffused spectra of TiO_2 powders were obtained for dry-pressed disc samples using a UV–Vis spectrophotometer (UV8500, Shimadzu, Japan). $BaSO_4$ was used as the reflectance standard in all the UV–Visible diffuse reflectance experiments.

Results and Discussion

Influence of Gliding Arc Plasma on Exposed $TiCl_3$ Solution

A purplish-red solution of $TiCl_3$ exposed to the plasma had its colour progressively vanishing, suggesting that the $TiCl_3$ is gradually converted into white suspended solid which could probably be TiO_2 as shown in Fig. 2.

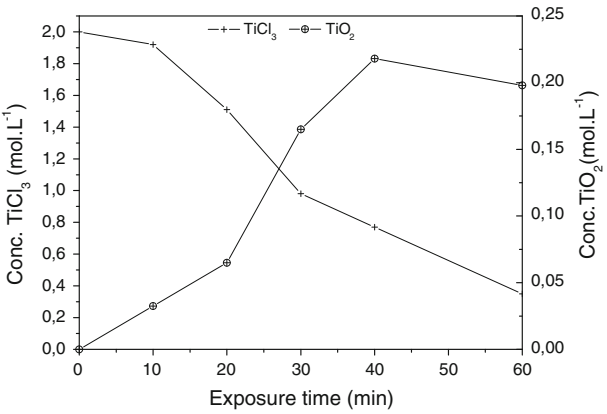

Fig. 2 Influence of exposure time on the reduction of $TiCl_3$ and the formation of TiO_2

These preliminary results may be illustrated by the oxidizing effect of the discharge and the following reaction could explain the formation of titanium dioxide:

$$TiCl_3 + OH^{\cdot} + H_2O \rightarrow TiO_2 + 3HCl \quad (14)$$

The $HO^{\cdot}$ radicals mainly formed in the arc will be the determining agents for the chemical reactions observed in the target solution. The formation of this radical has previously been confirmed by spectroscopic measurements and results from electron impact on water (Eqs. 15, 16) [9]. However, the $HO^{\cdot}$ radicals can also be formed by water reduction in a liquid phase due to hydrated electrons [19].

$$H_2O + e^- \rightarrow H^{\cdot} + HO^{\cdot} + e^- \quad (15)$$

$$H_2O + e^- \rightarrow H^+ + HO^{\cdot} + 2e^- \quad (16)$$

This is an essential feature and confirms previous observations on the plasma-chemical properties of the gliding discharge relevant to the oxidizing degradation of organic wastes.

XRD Analysis

Typical XRD patterns of the plasma-synthesised titanium oxide powder are depicted in Fig. 3. The assignment of XRD peaks showed that the obtained powder is a mixture of anatase and rutile form of TiO_2. The diffraction peaks of metallic titanium were not detected. Furthermore, it is interesting to find that TiO_2 nanoparticles synthesised by gliding arc plasma consist of both anatase and rutile phases since it has been shown that a mixture of the two phases improve much more photocatalytic activity than each pure phase [20].

FTIR Analysis

The FTIR spectrum of the plasma-synthesized is shown in Fig. 4. The broad peak between 3,100 and 3,600 cm^{-1} is assigned to the stretching vibrations of the OH groups of adsorbed water. The peaks in the range of 1,620–1,630 cm^{-1} are attributed to the bending vibrations of surface-adsorbed molecular water. The main peaks in the range 400–800 cm^{-1} correspond to Ti–O and Ti–O–Ti stretching vibrations [21, 22] and confirm the presence of TiO_2 phases in the synthesised material.

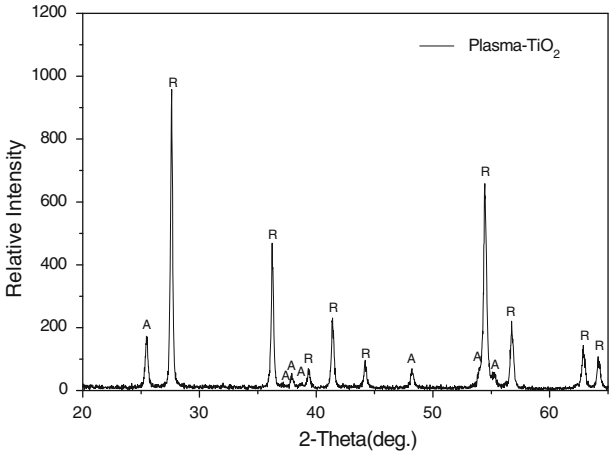

Fig. 3 XRD powder patterns of gliding arc plasma-synthesized TiO_2 (*A*: anatase, *R*: rutile)

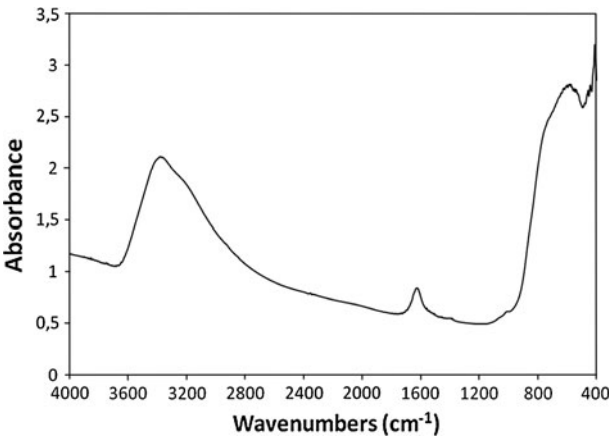

Fig. 4 FTIR spectrum of TiO_2 synthesized by gliding arc plasma

Surface Morphology of Plasma Synthesized TiO_2

Scanning electron microscopy analysis of plasma synthesized TiO_2 (Fig. 5a, b) shows that the morphology of the particles consists of anisotropic rods. It is also seen that these rods consist of porous agglomerates. This could be due to the permanent stirring of target solution. On the other hand, the sample presents several macropores structures which could allow the diffusion of pollutants and should increased the photo-degradation of organic molecules. This result is confirmed by the TEM micrographs (Fig. 5c, d) that show that these rods have length of 50–100 nm and a diameter of 5–15 nm.

Textural Properties of Plasma Synthesized TiO_2

The N_2 adsorption–desorption isotherms of a typical plasma-TiO_2 sample are shown in Fig. 6. The sample exhibits type IV isotherm with a hysteresis loop in the relative pressure

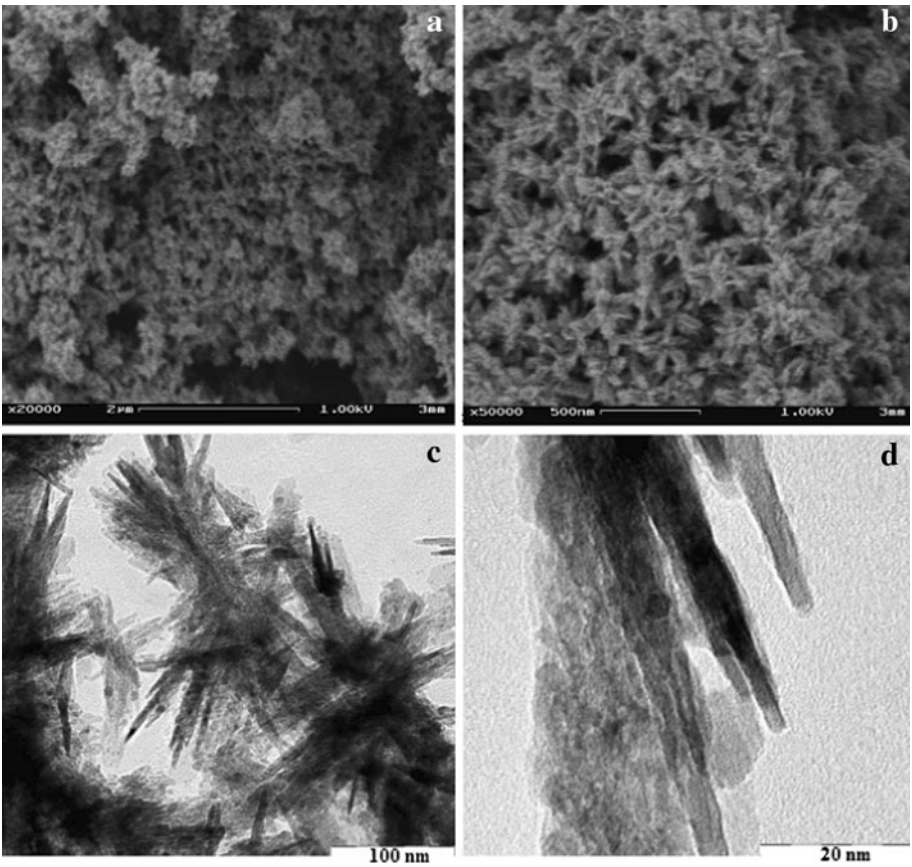

Fig. 5 SEM (**a, b**) and TEM (**c, d**) micrographs of plasma-synthesized TiO_2 showing the *rod shapes* of particles

range of 0.8–1.0, indicating the presence of inhomogeneous mesopores [23]. The inset figure represents the pores size distribution curve calculated from the desorption branch by the BJH method and displays several maxima in a range of 2–50 nm. Furthermore, the observed hysteresis loop approach $P/P_0 = 1$ suggests the presence of several macropores (>50 nm) [24]. This heterogeneity in the pores size distribution is correlated with the variable particles size as shown by TEM micrographs. Considering the morphology of the nanorods observed on these micrographs, the smaller pores (<10 nm) could correspond to the pores inside the nanorods, while the larger pores (10–100 nm) can be attributed to the aggregation of the nanorods [24].

The porous nanorods have a BET surface area of 158 $m^2\ g^{-1}$. Since sorption is one of the controlling factors of the catalytic oxidation reaction [25], the high surface area of plasma-TiO_2 particles is crucial for its use as photocatalyst.

UV–Vis Diffuse Spectroscopy

The UV–Vis absorbances of plasma-synthesized TiO_2 nanopowders are depicted in Fig. 7 and are compared to that of commercial TiO_2. As shown on this figure, it is evident that

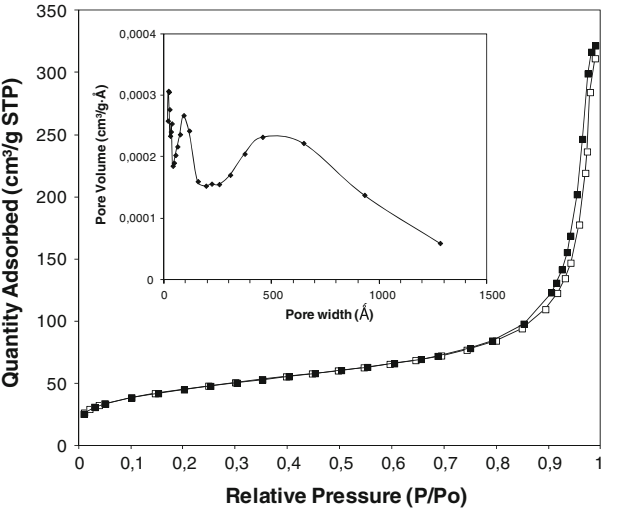

Fig. 6 N_2 adsorption–desorption isotherms of the plasma-TiO_2 sample (*empty square*: adsorption, *full square*: desorption); *inset*: pore size distribution curve

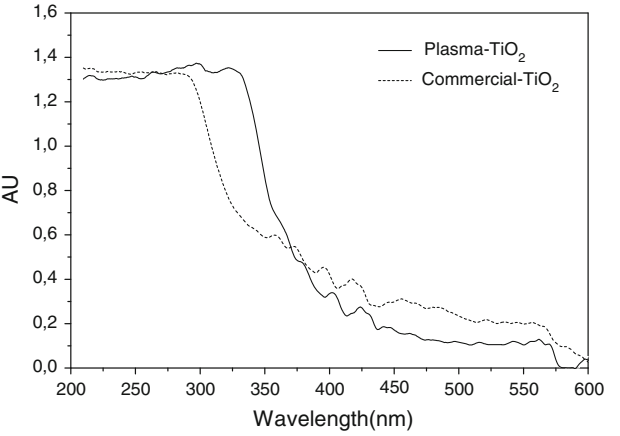

Fig. 7 UV–Vis diffuse reflectance spectra of commercial and plasma-synthesized TiO_2

UV–absorption edge of plasma-synthesized TiO_2 nanopowders extends to high wavelengths (towards visible region), which is useful for improving the photo-absorption and photo catalytic performance of TiO_2 under visible light. This curve shows that unlike commercial TiO_2, TiO_2 synthesised by glidarc absorbs in the range of 200–375 nm. In that case, it is possible that the plasma-TiO_2 was doped by nitrogen atoms during the synthesis process, since TiO_2 doped with non metallic atoms like nitrogen shows high photocatalitic activity under visible light. This result allows us to optimise the photocatalytic properties of TiO_2 because nearly 5 % of the sunlight energy emitted which reaches the surface of the earth is in the range of UV–A.

Conclusion

A nano-size TiO_2 adequate for sunlight photocatalysts have been successfully prepared through electric discharges of the gliding arc type applied on $TiCl_3$ solution. The use of

non-thermal quenched plasmas at atmospheric pressure favours the formation of active species and free radicals which confer to that process its particular chemical properties. The plume of quenched plasma licks a target solution and its species react at the target-plasma interface oxidizing the $TiCl_3$ precursor for give the nanorods of TiO_2. The resulting nanorods of TiO_2 are a mixture of anatase and rutile phase as shown by XRD analysis. Beside this feature, the high porosity of plasma-TiO_2 as depicted by SEM, TEM and BET results, can significantly improve the catalytic activity of the synthesised material. UV–Vis analysis showed that the typical plasma-TiO_2 has a high absorption wavelength (low band gap energy) as compared to a commercial TiO_2. This work establishes that gliding arc plasma is one of the most effective ways to synthesise TiO_2 nanorods that can be used as photocatalyst in the degradation of organic pollutant under visible light.

Acknowledgments The authors are grateful to the National Council for Scientific and Technological Development (CNPq), Brazil, and the academy of sciences for the developing world (TWAS), for Sandwich Postgraduate Fellowship awarded to E. Acayanka (No. 190102/2011-0). They are also grateful to the UCL fellowship program "coopération au développement" for financing A. Tiya Djowe's research visits in Belgium. Finally, the authors thank Pr. J.-L. Brisset of Université de Rouen for plasma reactor support and Mr. P. Eloy of Université catholique de Louvain for help in XRD and TEM analysis.

References

1. Jiaguo Y-U, Zhao X, Zhao Q (2000) Effect of surface structure on photocatalytic activity of TiO_2 thin films prepared by sol–gel method. Thin Solid Films 379:7–14
2. Zhou X-F, Chu D-B, Wang S-W, Lin C-J, Tian Z-Q (2002) New route to prepare nanocrystalline TiO_2 and its reaction mechanism. Mater Res Bull 37:1851–1857
3. Czernichowski A (1994) Gliding arc application to engineering and environmental control. Pure Appl Chem 66:1301–1310
4. Njoyim E, Ghogomu P, Laminsi S, Nzali S, Doubla A, Brisset J-L (2009) Coupling gliding discharge treatment and catalysis by oyster shell powder for pollution abatement of surface waters. Ind Eng Chem Res 48(22):9773–9780
5. Brisset J-L, Moussa D, Doubla A, Hnatiuc E, Hnatiuc B, Kamgang Youbi G, Herry J-M, Naïtali M, Bellon-Fontaine M-N (2008) Chemical reactivity of discharges and temporal post-discharges in plasma treatment of aqueous media: examples of gliding arc discharge treated solutions. Ind Eng Chem Res 47:5761–5781
6. Kamgang Youbi G, Herry J-M, Bellon-Fontaine M-N, Brisset J-L, Doubla A, Naïtali M (2007) Evidence of temporal postdischarge decontamination of bacteria by gliding electric discharges: application to *Hafnia alvei*. Appl Environ Microbiol 73:4791–4796
7. Doubla A, Laminsi S, Nzali S, Njoyim E, Kamsu-Kom J, Brisset J-L (2007) Organic pollutants abatement and biodecontamination of brewery effluents by a non-thermal quenched plasma at atmospheric pressure. Chemosphere 69:332–337
8. Laminsi S, Acayanka E, Nzali S, Teke Ndifon P, Brisset J-L (2012) Direct impact and delayed post-discharge chemical reactions of FeII complexes induced by non-thermal plasma. Desal Water Treat 37:1–8
9. Benstaali B, Boubert P, Cheron B, Addou A, Brisset J-L (2002) Density and rotational temperature measurements of the NO and OH radicals produced by a gliding arc in humid air and their interaction with aqueous solutions. Plasma Chem Plasma Process 22:553–571
10. Locke B-R, Sato M, Sunka P, Koffmann M-R, Chang J-S (2006) Electrohydraulic discharge and non-thermal plasma for water treatment. Ind Eng Chem Res 45:882–905
11. Burlica R, Kirkpatrick M-J, Finney W-C, Clark R-J, Locke B-R (2004) Organic dye removal from aqueous solution by glidarc discharges. J Electrost 62:309–321
12. Benstaali B, Cheron B, Addou A, Brisset J-L (1999) Spectral investigation of a gliding arc in humid air: a key for chemical applications. In: Proceedings of IUPAC congress on ISPC-14 (International symposium on plasma chemicals, Praga, Czech Republic), 2, pp 939–944
13. Brisset J-L, Hnatiuc E (2012) Peroxynitrite: a re-examination of the chemical properties of non-thermal discharges burning in air over aqueous solutions. Plasma Chem Plasma Process 32:655–674

14. Doubla A, Bouba L, Fotso M, Brisset J-L (2007) Plasmachemical decolourization of bromothymol blue by gliding arc discharge. Dyes Pigm 77:118–124
15. Pascal S, Moussa D, Hnatiuc E, Brisset J-L (2010) Plasma chemical degradation of phosphorous-containing warfare agents stimulants. J Hazard Mater 175:1037–1041
16. Moussa D, Brisset J-L (2003) Disposal of spent tributylphosphate by gliding arc plasma. J Hazard Mater 102:189–200
17. Brunauer S, Emmet P-H, Teller E (1938) Adsorption of gases in multimolecular layers. J Am Chem Soc 60:309–319
18. Barret E-P, Joyner L-G, Halenda P-H (1951) The determination of pore volume and area distributions in porous substance. I. Computations from nitrogens isotherms. J Am Chem Soc 73:373–380
19. Mariotti D, Patel J, Svrcek V, Maguire P (2012) Plasma–liquid interactions at atmospheric pressure for nanomaterials synthesis and surface engineering. Plasma Process Polym 9:1074–1085
20. Lopez T, Gomez R, Sanchez E, Tzompantzi F, Vera L (2001) Photocatalytic activity in the 2,4-dinitroaniline decomposition over TiO_2 sol-gel derived catalysts. J Solgel Sci Technol 22:99–107
21. Jensen H, Soloviev A, Li Z, Sogaard E-G (2005) XPS and FTIR investigation of the surface properties of different prepared titania nano-powders. Appl Surf Sci 246:239–249
22. Yu J, Su Y, Cheng B, Zhou M (2006) Effects of pH on the microstructures and photocatalytic activity of mesoporous nanocrystalline titania powders prepared via hydrothermal method. J Mol Catal A: Chem 258:104–112
23. Brunauer S, Deming L-S, Deming W-S, Teller E (1940) On a theory of the van der Waals adsorption of gases. J Am Chem Soc 62:1723–1732
24. Donga P, Wanga Y, Liu B, Guoa L, Huanga Y, Yin S (2012) Effect of hydrothermal reaction time on morphology and photocatalytic activity of $H_2Ti_3O_7$ nanotubes obtained via a rapid synthesis route. Appl Surf Sci 258:7052–7058
25. Watts R-J, Foget M-K, Kong S-H, Teel A-L (1999) Hydrogen peroxide decomposition in model subsurface systems. J Hazard Mater 69:229–243